Supporting Information

Metabolic Modulation-Driven Self-Reinforcing Pyroptosis-STING Nanoadjuvant for Potentiated Metalloimmunotherapy

1.1 Experimental section

Materials

Cobalt acetylacetonate ($Co(C_5H_7O_2)_2$) was purchased from Shanghai Debao Biotechnology Co., Ltd. Ammonium fluoride (NH_4F) and dibenzyl ether (95%) were purchased from Alfa Aesar (China) Chemical Co., Ltd. Dodecanol ($C_{12}H_{26}O_2$, 93%), oleic acid (90%), and oleylamine (95%) were purchased from Beijing Anheuser-Busch InBev Science Co., Ltd. 1,3-Diphenylisobenzofuran (DPBF) was purchased from Macklin Biochemical Technology Co., Ltd. 3,3',5,5'-Tetramethylphenyldiamine (TMB) was purchased from Beijing J&K Science Co., Ltd. Hydrogen peroxide (H_2O_2, 30%) was purchased from Shanghai Lingfeng Chemical Reagent Co., Ltd. All the chemicals were of analytical grade and used without further purification. An adenosine triphosphate (ATP) content determination kit (BC0300) was purchased from Beijing Solarbio Technology Co., Ltd. Glucose Dehydrogenase (LDH) content assay kit (C0016) and mitochondrial membrane potential test kit (JC-1, C2006) were purchased from Beyotime Biotechnology Co., Ltd. Glucose oxidase (GOx) and DSPE-PEG_{2000}-NH_2 kits were purchased from ShangHai Ponsure Biotech, Inc. Anti-HMGB1 rabbit mAb (ab79823), anti-CRT rabbit mAb (ab2907), anti CD3-FITC (Biolegend, clone 17A2, Catalog: 100204), anti-CD4-APC (Biolegend, clone GK1.5, Catalog: 100412), anti-CD8-PE (Biolegend, clone 53-6.7, Catalog: 100708), anti-CD11c-FITC (Biolegend, clone N418, Catalog: 117306), anti-CD80-APC (Biolegend, clone 16-10A1, Catalog: 104714), anti-CD86-PE (Biolegend, clone GL-1, Catalog: 105008), anti-F4/80-FITC (Biolegend, 2 clone QA17A29, Catalog: 157310), anti-CD206-APC (Biolegend, clone C068C2, Catalog: 141708), anti-CD11b-PE (Biolegend, clone M1/70, Catalog: 101280), anti-CD44-PE (Biolegend, clone IM7, Catalog: 103010), anti-CD8-PerCP (Biolegend, clone 53-6.7, Catalog: 100732), anti-Foxp3-PE (Biolegend, clone MF-14, Catalog: 126404), and anti-CD62L-APC (Biolegend, clone MEL-14, Catalog: 104450) were obtained from Biolegend and diluted at 1:300 for cell staining. Mouse TNF-α (Cat No. HJ207; Epizyme, Shanghai, China) and IFN-γ (Cat No. HJ170;

Epizyme, Shanghai, China) ELISA kit were purchased from Shanghai Epizyme (china). Mouse IFN-β ELISA kit (JL20268) was purchased from Shanghai Jianglai Biology Co, Ltd. ELISA kits for IL-1β (ED-20174) was purchased from Lun Changshuo Biological Technology Co., Ltd. GenScript YoungPAGE™ Precast Gels (M00928) was obtained from GenScript Biotech Corporation. anti-Phospho-Histone H2A. 11263-1-AP), SOX2 (Proteintech, Catalog: 11064-1-AP), Cleaved Caspase-1 rabbit mAb (CST, 89332), anti-Caspase-1 antibody (Abcam, AB138483), cleaved gasdermin D rabbit mAb (CST, 10137), anti-GSDMD (Abcam, AB219800) and anti-TBK1/NAK (E8I3G) (CST, Catalog: 38066), anti-phospho-TBK1/NAK (Ser172) (D52C2) XP® (CST, Catalog: 5483), anti-IRF-3 (D6I4C) (D6O1M) (CST, Catalog: 29047), anti-STING (D2P2F) (CST, Catalog: 13647), anti-phospho-STING (Ser366) (E9A9K) (CST, Catalog: 50907), anti-beta-Tubulin (Proteintech, Catalog: 10094-1-AP), anti-GAPDH (Proteintech, Catalog: 10494-1-AP), and FDR007 goat anti-rabbit lgG (H + R) HRP secondary antibody (Fudebio, Hangzhou, China) was obtained and diluted at 1:1000 for Western blotting (WB) analysis. The signals were developed using FD8020 FDbio-Dura ECL (Fudebio, Hangzhou, China). RPMI-1640 medium was purchased from Thermo Fisher Scientific Inc. The aqueous solution used in the experiment was prepared from deionized water from a Milli-Q water purification system.

Synthesis of CoF_2 nanoparticles (NPs)

Briefly, 1 mmol of cobalt acetylacetonate, 2 mmol of NH_4F, 2 g of 1,2-dodecanediol, 20 mL of diphenyl ether, 2 mL of oleylamine (OE) and 2 mL of oleic acid (OA) were added to a three-necked flask. The mixture was heated to 120 °C under N_2 and maintained for half an hour under magnetic stirring. Then, the mixture was heated to 280 °C and stirred for 1 h, after which the CoF_2 was washed three times with cyclohexane and ethanol.

Synthesis of GOCoF_2 NPs

The synthesized CoF_2 NPs were modified. 30 mg of DSPE-PEG_{2000}-NH_2 and 5 mg of CoF_2 NPs were dissolved in 15 mL of dichloromethane and treated with ultrasonic waves in a water bath for 30 mins, after which the dichloromethane was removed via rotary evaporation. Then, the PEGylated CoF_2 was ultrasonically cleaned three times with deionized water and finally fixed to 10 mL. Finally, 3 mg of GOx was added, and the mixture was vortexed at room temperature for 1 hour, washed three times with deionized water, and stored at 4 °C for use.

Characterization

The morphology of the samples was characterized by transmission electron microscopy (TEM, FEITF20). Elemental mapping was performed by TEM (TALOS 200X). The chemical composition and crystallography of the samples were characterized by X-ray diffraction (XRD, Panalytical Empyrean) with Cu Kα radiation (λ = 1.54056 Å). The phase analysis was examined by X-ray photoelectron spectroscopy (XPS). UV-vis-NIR absorption spectra were recorded by UV-vis-NIR spectrophotometer (PerkinElmer Lambda 750). The concentration of Co element was determined by inductively coupled plasma optical emission spectrometry (ICP-OES). Fourier transform infrared spectrometer (FT-IR) imaging was carried out by FT-IR Spectrometer (V70 & Hyperion 1000, Bruker, Billerica, USA). Dynamic light scattering (DLS) and zeta potential of the nanoparticles were recorded using MAL VERN ZEN3690.

Determination of $GOCoF_2$ activity

In order to detect the ability of the CoF_2 NPs to catalyze H_2O_2. Specifically, to detect superoxide anion ($O_2^{\bullet-}$), first, 10 μL of the DPBF (1 mg/mL) probe and 20 μL of H_2O_2 (1 mmol/L) were dissolved in 920 μL of deionized water, and finally, 50 μL of CoF_2 (5 mg/mL) was added to immediately record the absorption peak at 420 nm. Subsequently, the ability of CoF_2 to produce $O_2^{\bullet-}$ and was assessed via the use of NBT probe, 15 μL of NBT in dimethyl sulfoxide (DMSO, 1 mg/mL), 50 μL of H_2O_2 (1 mmol/L) were dissolved in 885 μL of deionized water, and finally, 50 μL of CoF_2 (5 mg/mL) was added to immediately record the absorption peak at 260 nm.

To detect •OH, first, 5 μL of TMB probe and 20 μL of H_2O_2 (1 mmol/L) were dissolved in 925 μL of deionized water, and finally, 50 μL of CoF_2 (5 mg/mL) was added to immediately record the absorption peak at 652 nm. In addition, OPD is also used to detect •OH, 20 μL of the OPD in deionized water (H_2O, 10.8 mg/mL), 50 μL of H_2O_2 (1 mmol/L) were dissolved in 880 μL of deionized water, and finally, 50 μL of CoF_2 (5 mg/mL) was added to immediately record the absorption peak at 430 nm.

To detect the ability of the $GOCoF_2$ NPs to catalyze glucose, in short, to detect $O_2^{\bullet-}$, first, 10 μL of DPBF (1mg/mL) probe and 10 μL of glucose (1 mol/L) were dissolved in 920 μL of deionized water, and finally, 50 μL of CoF_2 (5 mg/mL) was added to immediately record the absorption peak at 420 nm. Subsequently, 15 μL of NBT in dimethyl sulfoxide (DMSO, 1 mg/mL), 10 μL of glucose (1 mol/L) were dissolved in 925 μL of deionized water, and finally, 50 μL of $GOCoF_2$ (5 mg/mL) was added to immediately record the absorption peak at 260 nm. To detect •OH, 5 μL of TMB probe and 10 μL glucose (1 mmol/L) were first dissolved in 925 μL of deionized water, and finally, 50 μL CoF_2 (5 mg/mL) was added, and the absorption peak at 652 nm was immediately recorded. In addition,

OPD is also used to detect •OH, 20 μL of the OPD in deionized water (H_2O, 10.8 mg/mL), 10 μL of glucose (1 mol/L) were dissolved in 920 μL of deionized water, and finally, 50 μL of $GOCoF_2$ (5 mg/mL) was added to immediately record the absorption peak at 430 nm.

Measurement of glucose

To measure glucose levels in cells, cells were lysed on ice and homogenized with lysis buffer, and the supernatant was obtained by centrifugation at 12,000 g for 5 min at 4 °C. The supernatant was collected, and glucose levels were measured using a glucose assay kit with O-toluidine (Beyotime: S020S) according to the manufacturer's instructions.

Cellular experiments

The H22 hepatoma cell line was cultured in RPMI 1640 medium containing 10% FBS (JYK-FBS-303, Jin Yuan Kang Biotechnology) and 1% penicillin-streptomycin in a standard cell culture environment (37 °C, 5% CO_2).

To study cytotoxicity and relative cell viability, a standard CCK8 (TargetMol, USA, C0005) assay was used for measurement. H22 cells were evenly plated in 12-well plates (10^5 cells per well) and cultured overnight at 37 °C. After different treatments (control, GOx, CoF_2, and $GOCoF_2$), the cells were incubated at 37 °C for 24 h. Then, CCK8 solution was added, and the mixture was incubated for 1.5 h. The cell suspension was transferred to a 96-well plate. The absorbance of each well at 490 nm was measured.

To detect cellular ROS, H22 cells were incubated with 100 μM $GOCoF_2$ for 6 h and then stained with DCFH-DA (10 μM) for 30 min according to the kit recommended protocol. Then, the cells were

washed with PBS and detected by flow cytometry. Afterwards, the cells were stained with DAPI for 15 min. Images were acquired via confocal microscopy (CLSM, Zeiss Axio-Imager LSM-800).

To determine the mitochondrial membrane potential, H22 cells (1×10^5/well) were seeded in 6-well plates, and the cells in different treatment groups (ctrl., GOx, CoF_2, and $GOCoF_2$) were incubated at 37 °C for 8 h. The mitochondrial membrane potential of the cells was detected via a JC-1 kit and flow cytometer (BD Accuri C6 flow cytometer).

To assess the stemness properties of H22 cells, 1×10^5 H22 cells per well were plated in 6-well plates. Cells from various experimental groups (Ctrl., GOx, CoF_2, and $GOCoF_2$) were incubated at 37°C for 24 hours, followed by staining with antibodies specific for stemness markers. Changes in stemness marker expression were subsequently analyzed using a BD Accuri C6 flow cytometer.

To determine ATP and LDH release, H22 cells (1×10^5/well) were seeded in 12-well plates, and cells in different treatment groups were incubated at 37 °C for 8 h. The supernatant was collected and treated with ATP and LDH according to the instructions. The samples were analyzed via microplate reader.

To detect CRT expression and HMGB1 release, H22 cells (1×10^5/well) were seeded in 12-well plates, and the cells in different treatment groups were incubated at 37 °C for 12 h. For HMGB1, the cells were washed with PBS, fixed with 4% paraformaldehyde, and transparentized with 0.1% Triton X-100 for 10 min. After incubation with 5% FBS for 0.5 h, the cells were incubated with an anti-HMGB1 antibody for 1 h and then incubated with an Alexa 488-conjugated secondary antibody for 45 min. Then, the cells were washed with PBS and detected via flow cytometry. For CRT, the cells were washed with PBS and fixed with 4% paraformaldehyde. After incubation with 5% FBS for 0.5 h, the cells were incubated with an anti-CRT antibody for 1 h and then an Alexa 488-conjugated

secondary antibody for 45 min. Then, the cells were washed with PBS and detected by flow cytometry.

A comet assay was used to detect DNA damage using a comet assay kit (Beyotime, CC2041S) according to the manufacturer's protocol. H22 cells were evenly dropped onto agarose electrophoresis slides and then immersed in 4 °C lysis buffer for 1 h. The slides were placed in a horizontal electrophoresis tank and electrophoresed at 25 V in a 4 °C refrigerator in the dark for 30 min. The slides were removed, and dried at 37 °C for 10 min, and stained with ethidium bromide (EB) solution, acridine orange (OA) solution, or DAPI solution, respectively, in the dark for 20 min. Electrophoresis images were captured via a confocal microscope.

Annexin V-FITC/PI was used to detect cell apoptosis and pyroptosis. H22 cells (1×10^5/well) were seeded in 6-well plates and treated with 100 μM $GOCoF_2$ for 12 h. Single cell suspensions were further obtained, stained with Annexin-FITC and PI, and analyzed by flow cytometry. Moreover, 2×10^4 H22 cells were uniformly seeded in a confocal dish, and the cell morphology was determined via confocal microscopy.

For mitochondrial morphology detection, biological transmission electron microscopy (TEM) was used. Briefly, H22 cells (1×10^5/well) were seeded in a dish and treated with 100 μM $GOCoF_2$ for 12 h. Fixation: The samples were pre-fixed with 2.5% glutaraldehyde and then re-fixed with 1% osmium tetroxide; Dehydration: acetone dehydration step by step, the concentration gradient of the dehydrating agent was 30%→50%→70%→80%→90%→95%→100% (100% concentration was changed 3 times); Infiltration: dehydrating agent and Epon-812 embedding agent were infiltrated in the ratio of 3:1, 1:1, and 1:3 respectively; Embedding: epon-812 pure embedding agent was embedded; Ultrathin sectioning: 60~90nm ultrathin sections were made with an ultrathin slicer and scooped onto a copper grid; Staining: first stain with uranyl acetate for 10~15min, then stain with lead citrate for

1~2 min, and stain at room temperature. Finally, images were obtained by TEM.

To detect the protein expression of cells by WB, H22 cells (1×10^7 per well) were seeded in 6-well plates, and the cells in different treatment groups were incubated at 37 ℃ for 24 h. Subsequently, the cells were washed twice with PBS, and the proteins were collected with cell lysis buffer for standard western blot analysis. Briefly, proteins were transferred to polyvinylidene fluoride (PVDF) membranes and then blocked with protein blocking buffer for 2 h. Primary antibodies against the corresponding proteins were incubated at 4 °C overnight, washed with PBST for half an hour, and incubated with secondary antibodies at room temperature for 2 h, and washed with PBST for half an hour. The signals were visualized by ECL using a ChemiDoc Touch imaging system (General Electric, AI600UV, USA).

Animal experiments

Female Balb/c mice (6-8 weeks old) and male Sprague-Dawley (SD) rats (200-250 g) were purchased from Jiangsu Huachuang Sino Pharma Tech Co., Ltd. All the animals were used in accordance with protocols approved by the Experimental Animal Center of Soochow University. To establish the subcutaneous H22 tumor model, H22 cells (2×10^6) suspended in 25 μL of PBS and 25 μL of Matrigel Matrix (MeisenCTCC - MS0302ZY) were injected subcutaneously into the right side of each Balb/c mouse. To establish the orthotopic N1S1 tumor model, N1S1 cells (6×10^6) suspended in 75 μL of PBS containing 30% Matrigel (Corning) were injected into the left lobe of the liver of each SD rat under anesthesia using a 25-gauge syringe needle. The $GOCoF_2$ dosage for all animal experiments was 5 mg/kg.

To evaluate the therapeutic effect of $GOCoF_2$, mice bearing subcutaneous H22 tumors (~120

mm^3) were randomly divided into 4 groups (n = 6) and received the following intratumoral injections: Group I, PBS; Group II: GOx; Group III: CoF_2; and Group IV: $GOCoF_2$. The intratumoral injection dose of GOx and CoF_2 was 5 mg kg^{-1}. Thereafter, the length and width of each tumor and the weight of each mouse were recorded every other day via a vernier caliper and an electronic scale, respectively. A tumor volume was calculated according to the formula: tumor volume = (width*width*length)/2. The mouse was considered dead when the tumor volume reached 1500 mm^3. In addition, two days after the intratumoral injection, one mouse in each group was randomly selected and sacrificed, and all the tumor was collected for H&E and immunohistochemical staining.

For transcriptome analysis, the mice bearing subcutaneous H22 tumors (~150 mm^3) were randomly divided into two groups, the control group (n = 4) and the $GOCoF_2$ (5 mg/kg, i.t. injection, n = 4) group. Tumor tissues were extracted for mRNA sequencing analysis after 7 days of treatment. Total cell mRNA was extracted with TRIzol reagent, and after verification of RNA integrity and purity, high-throughput sequencing of mRNA was performed at Suzhou Jinweizhi Technology Co., Ltd. Statistical analysis of the significant differential expression of genes was performed by $\log2|FC| \geq 1.5$ and q value (FDR, p adj) ≤ 0.05. p value ≤ 0.05 was considered significant for GO enrichment, and q value ≤ 0.05 was considered significant for KEGG enrichment.

To evaluate the immune status after $GOCoF_2$ treatment, mice bearing subcutaneous H22 tumors (~120 mm^3) were randomly divided into two groups (n = 5) and received the following intratumoral injections: Group I, PBS; Group II: $GOCoF_2$ (5 mg/kg, i.t. injection). H22 mice receiving different treatments were euthanized on day 8, and tumor tissues and proximal inguinal lymph nodes were carefully removed, suspended and cut into pieces to obtain single-cell suspensions. To further analyze the immune effects, the cells were stained with anti-CD3-FITC, anti-CD8-PE, anti-CD80-APC, anti-

CD11b-PE, anti-CD11c-FITC, anti-F4/80-FITC, and anti-CD86-PE antibodies (BioLegend). Immunological parameters were evaluated by flow cytometry.

To evaluate whether $GOCoF_2$ enhances the therapeutic effect of α-PD-1, mice bearing subcutaneous H22 tumors (~120 mm^3) were randomly divided into 4 groups (n = 6) and received the following treatments: Group I, PBS; Group II: α-PD-1 (0.1 mg/mL, 200 μL, i.v. injection); Group III: $GOCoF_2$; and Group IV: $GOCoF_2$ (5 mg/kg, i.t. injection) + α-PD-1 (0.1 mg/mL, 200 μL, i.v. injection). Tumor size was measured every 2 days, and tumor volume was calculated according to the formula tumor volume = (width*width*length)/2. The mice were considered dead when the tumor volume reached 1500 mm^3. In addition, two days after intratumoral injection, one mouse in each group was randomly selected and sacrificed, and the tumors were collected for H&E and immunohistochemical staining.

To evaluate the TACE effect of Lipiodol + $GOCoF_2$ on orthotopic N1S1 hepatocellular carcinoma tumors (~250 mm^3), 15 rats bearing orthotopic N1S1 hepatocellular carcinoma tumors (~250 mm^3) were randomly divided into three groups (n = 5) and treated as follows: Group I, control group; Group II, transarterial embolization (Lipiodol); Group III, transarterial embolization (Lipiodol + $GOCoF_2$); On day 0, rats in Group II and Group II were treated with transarterial embolization with Lipiodol, Lipiodol + $GOCoF_2$, respectively. The injection dose of GOx and $GOCoF_2$ were 200 μL, 5 mg kg^{-1}. The tumor volume of each group of rats was recorded on a 7.0-Tesla small animal MR scanner (Bruker Pharmascan, Ettlingen, Germany) on days 0, 4, 7, and 14 after treatment. The tumor volume (V) was calculated based on the tumor echogenicity in the superior-inferior (SI) and lateral-medial (LM) as well as anterior-posterior (AP) planes as follows: V (mm^3) = 3π/4×1SI/2×1LM/2×1AP/2. To further evaluate the therapeutic effect, one rat in each group was

killed on day 8, and the tumor tissues were collected for H&E and immunohistochemical staining.

Statistical analysis

The experimental results are expressed as mean ± SD and analyzed by GraphPad Prism 8 software. The independent sample t test was used for comparison between two groups, and one-way analysis of variance (ANOVA) was used for multiple comparisons among three or more groups; *$p < 0.05$, **$p < 0.01$, ***$p < 0.001$, ****$p < 0.0001$.

Supporting Figures

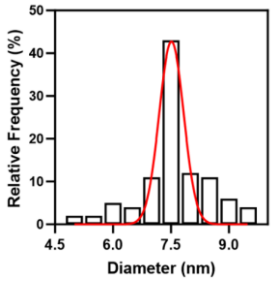

Figure S1. Diameter distribution of CoF_2 NPs.

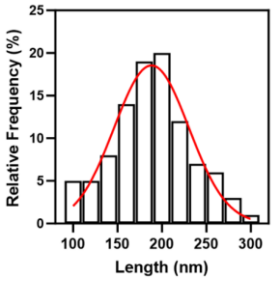

Figure S2. Length distribution of CoF_2 NPs.

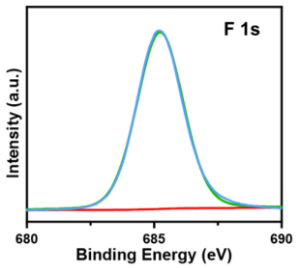

Figure S3. XPS spectra of F 1s after the catalytic reaction.

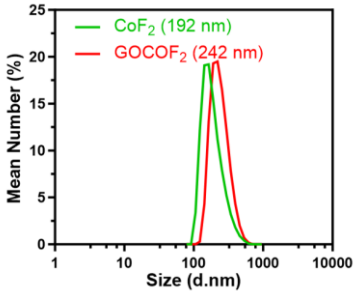

Figure S4. DLS results of the CoF_2 and $GOCoF_2$ NPs.

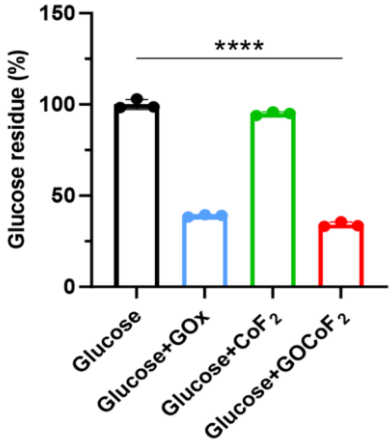

Figure S5. The glucose kit measures the ability of GOx and $GOCoF_2$ to consume glucose.

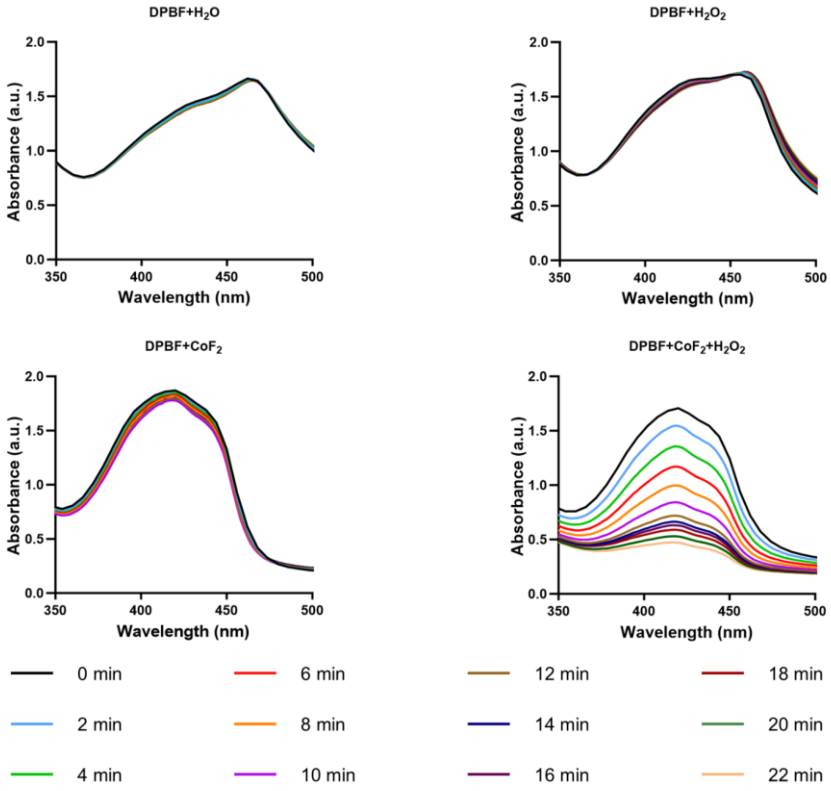

Figure S6. Individual time-dependent oxidation curves of DPBF by CoF_2 NPs under H_2O_2 condition.

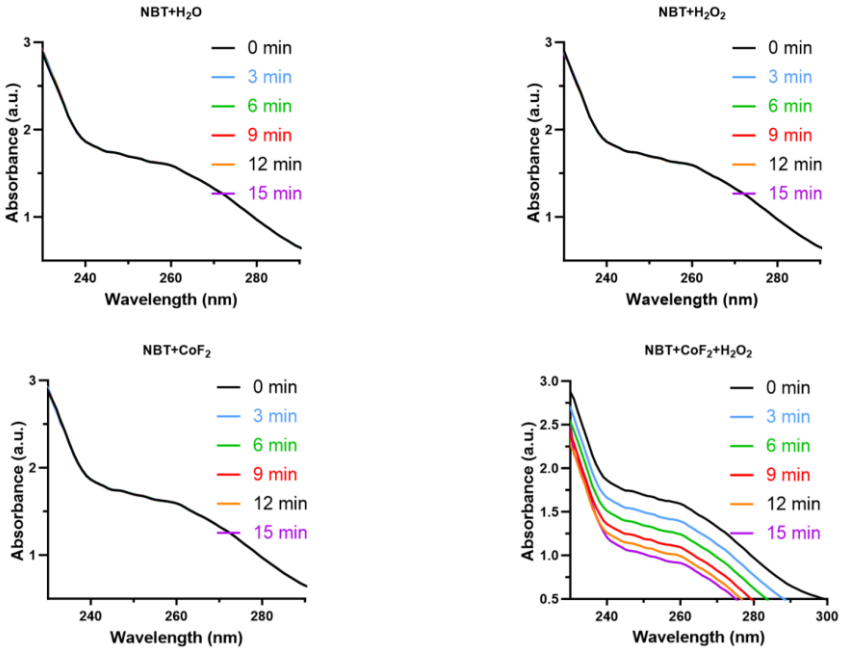

Figure S7. Time-dependent UV absorption of NBT after different treatments.

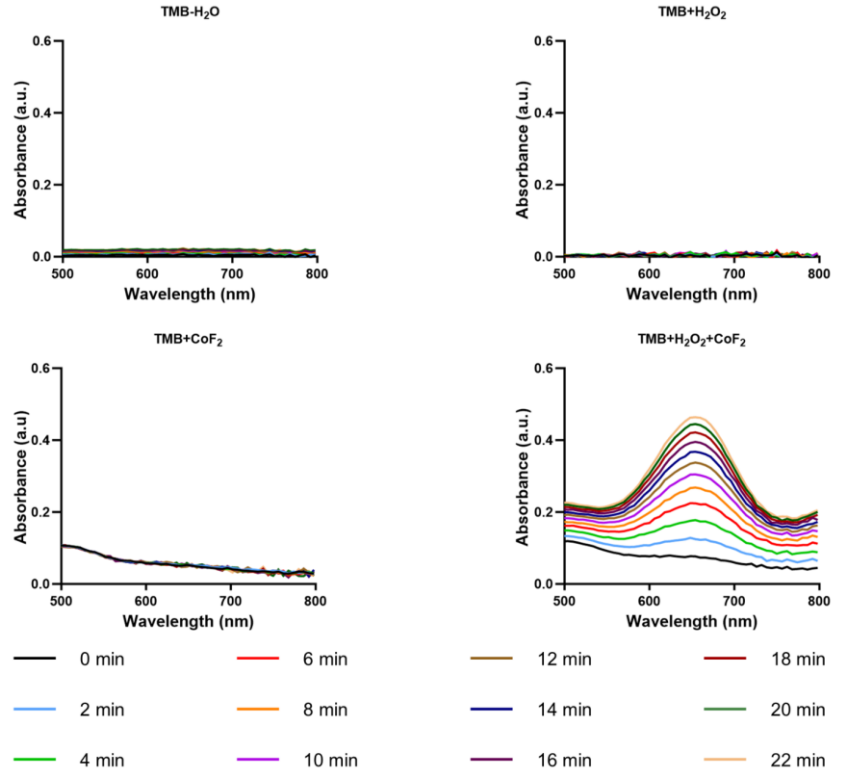

Figure S8. CoF_2 Individual time-dependent oxidation curves of the TMB probe by the CoF_2 NPs under H_2O_2 condition.

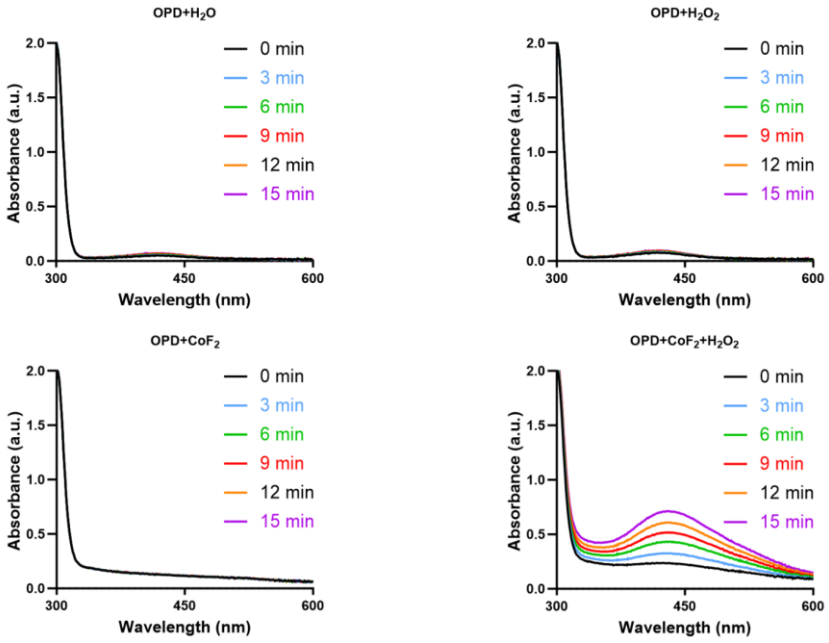

Figure S9. Time-dependent UV absorption of OPD after different treatments.

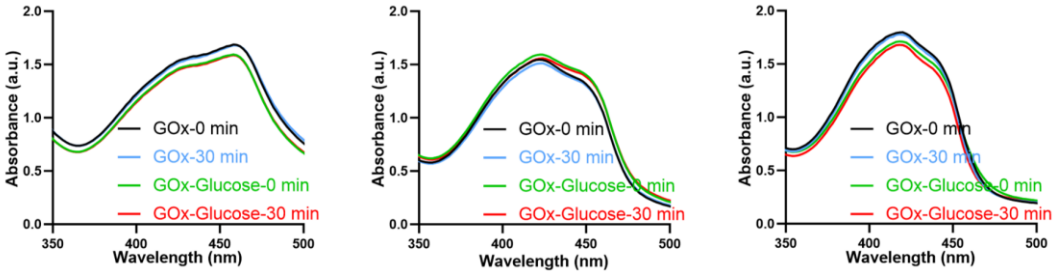

Figure S10. Individual time-dependent oxidation curves of DPBF by the CoF_2 NPs under glucose.

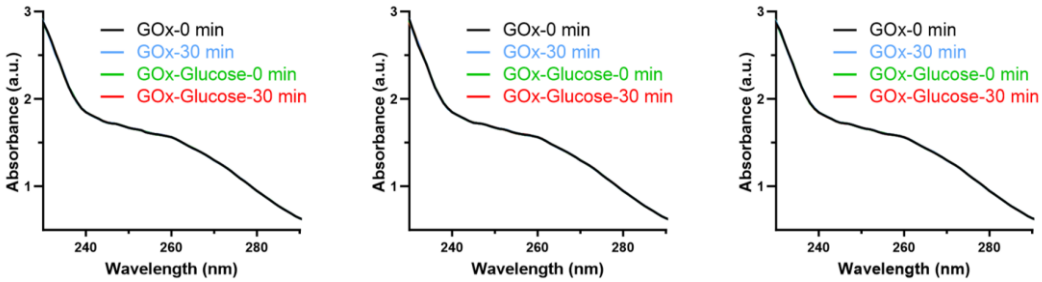

Figure S11. Individual time-dependent oxidation curves of NBT by the CoF_2 NPs under glucose.

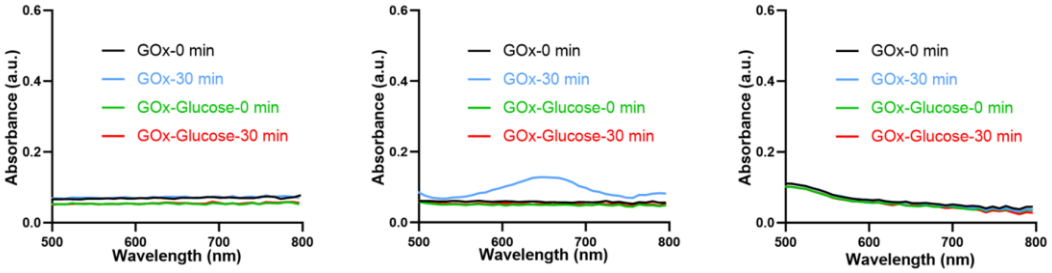

Figure S12. Individual time-dependent curves of •OH generation efficiency of $GOCoF_2$ NPs under glucose using TMB probe.

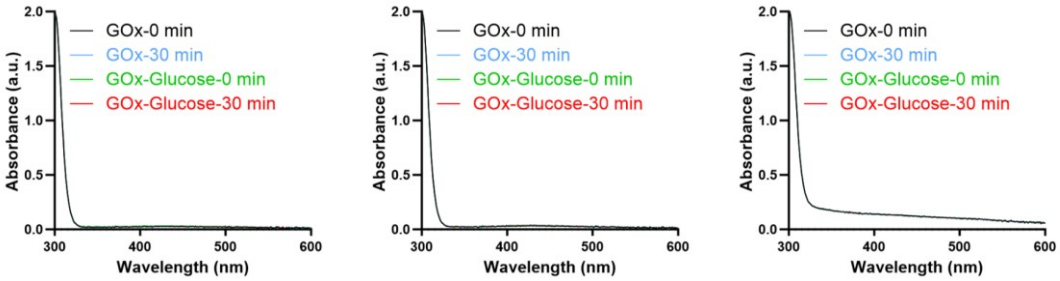

Figure S13. Individual time-dependent curves of •OH generation efficiency of $GOCoF_2$ NPs under glucose using OPD probe.

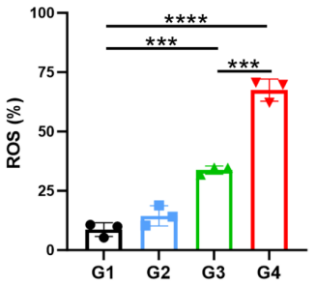

Figure S14. quantification of H22 cell ROS after various treatments. G1: Ctrl., G2: GOx, G3: CoF_2, G4: $GOCoF_2$.

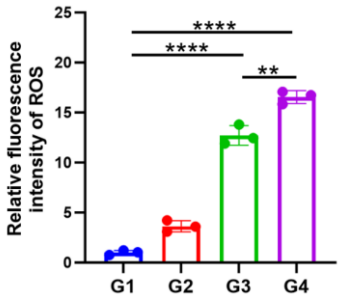

Figure S15. Quantitative analysis of the fluorescence intensity of intracellular ROS after various treatments. G1: Ctrl., G2: GOx, G3: CoF_2, G4: $GOCoF_2$.

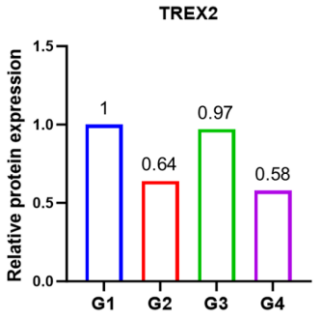

Figure S16. Quantitative analysis of Relative protein expression levels depicted in **Figure 3L**.

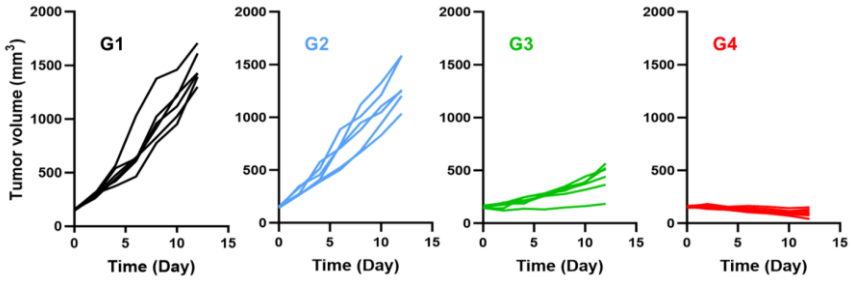

Figure S17. Individual growth curves of H22 tumors after various treatments. G1: Ctrl., G2: GOx, G3: CoF_2, G4: $GOCoF_2$.

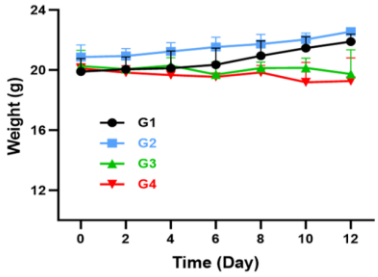

Figure S18. Changes in the body weights of tumor-bearing mice after different treatments. G1: Ctrl., G2: GOx, G3: CoF_2, G4: $GOCoF_2$.

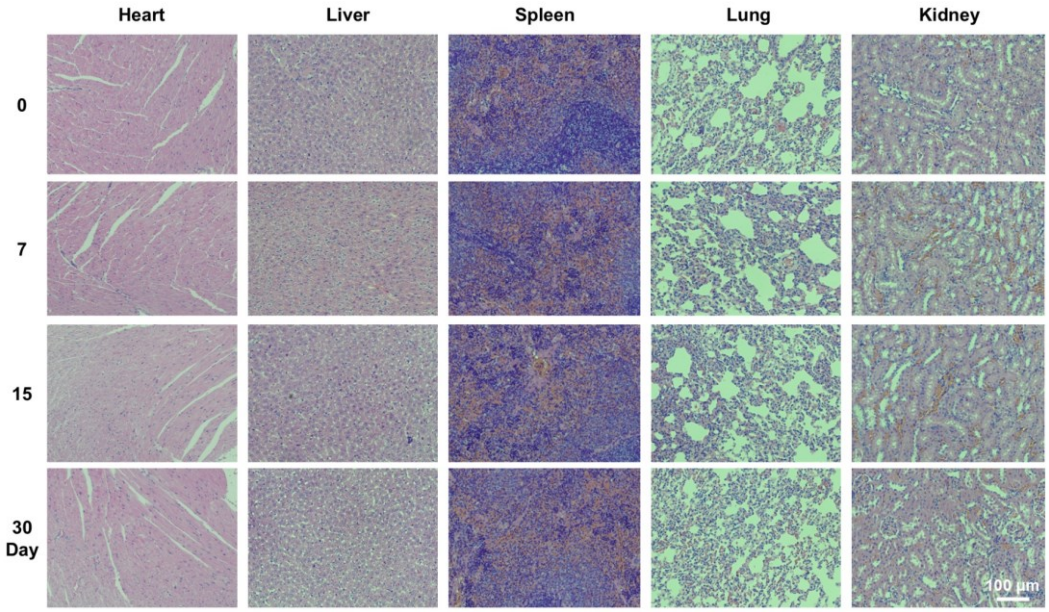

Figure S19. H&E-staining of the main organs, including heart, liver, spleen, lung, and kidney, from $GOCoF_2$ treatment.

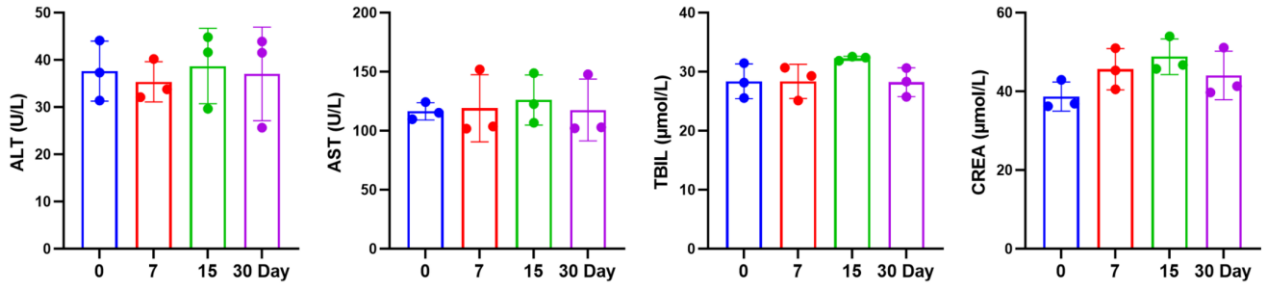

Figure S20. Blood biochemistry data of the mice treated with $GOCoF_2$ at various time points (0, 3, 7, 15, and 30 Days). Alanine aminotransferase (ALT), aspartate aminotransferase (AST), total

bilirubin (TBIL), creatinine (CREA).

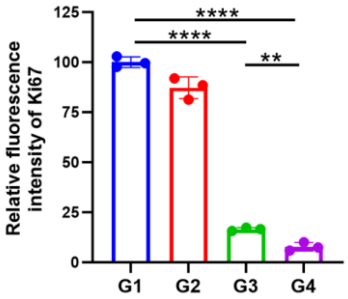

Figure S21. Quantitative analysis of the fluorescence intensity of Ki67 after various treatments. G1: Ctrl., G2: GOx, G3: CoF_2, G4: $GOCoF_2$.

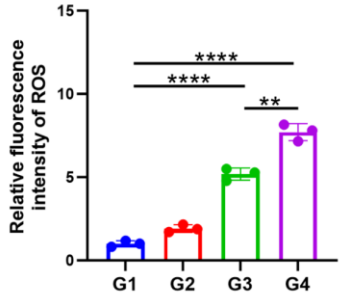

Figure S22. Quantitative analysis of the fluorescence intensity of ROS in tumor tissues after various treatments. G1: Ctrl., G2: GOx, G3: CoF_2, G4: $GOCoF_2$.

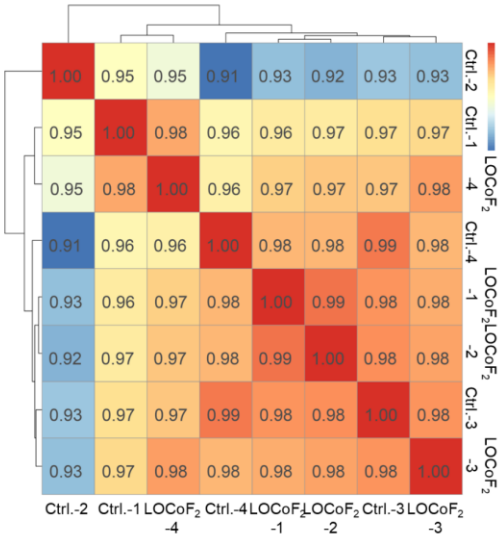

Figure S23. Unsupervised hierarchical clustering of the RNA-Seq data from the control and $GOCoF_2$ groups.

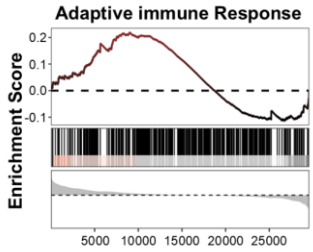

Figure S24. GSEA analysis showed the gene sets of Adaptive immune Response signaling pathway.

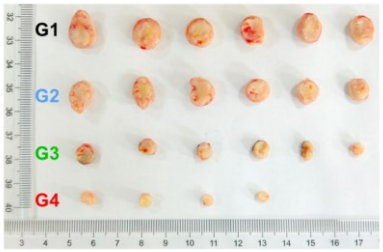

Figure S25. Images of H22 primary tumor-bearing mice 10 days after various treatments. G1: Ctrl., G2: α-PD-1, G3: $GOCoF_2$, G4: $GOCoF_2$ + α-PD-1.

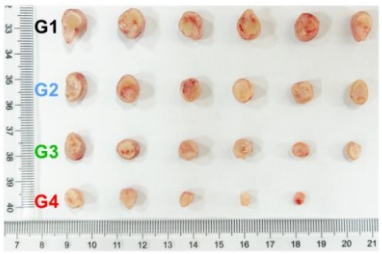

Figure S26. Images of H22 distant tumor-bearing mice at 10 days after various treatments. G1: Ctrl., G2: α-PD-1, G3: $GOCoF_2$, G4: $GOCoF_2$ + α-PD-1.

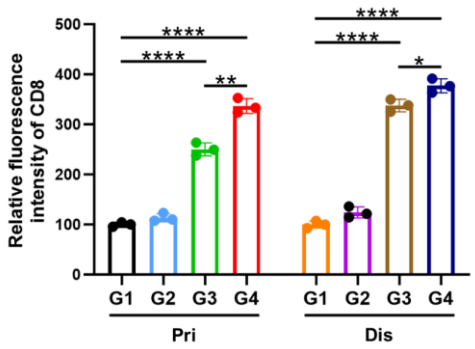

Figure S27. Quantitative analysis of the fluorescence intensity of CD8 in tumor tissues after various treatments. G1: Ctrl., G2: α-PD-1, G3: $GOCoF_2$, G4: $GOCoF_2$ + α-PD-1.

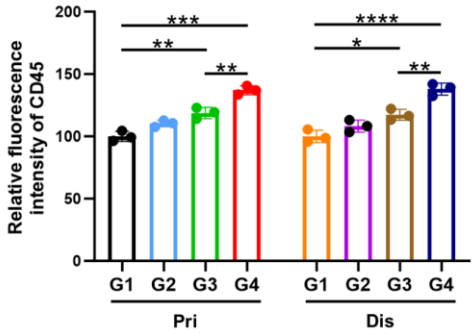

Figure S28. Quantitative analysis of the fluorescence intensity of CD45 in tumor tissues after various treatments. G1: Ctrl., G2: α-PD-1, G3: $GOCoF_2$, G4: $GOCoF_2$ + α-PD-1.

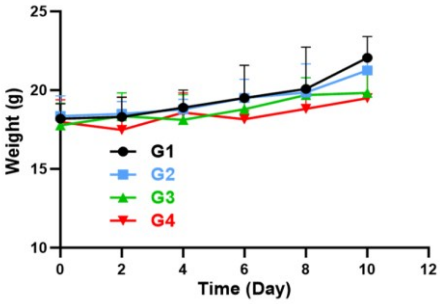

Figure S29. Changes in the body weights of tumor-bearing mice after different treatments. G1: Ctrl., G2: α-PD-1, G3: $GOCoF_2$, G4: $GOCoF_2$ + α-PD-1.

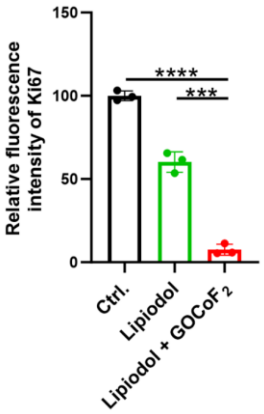

Figure S30. Quantitative analysis of the fluorescence intensity of Ki67 in tumor tissues after various treatments.

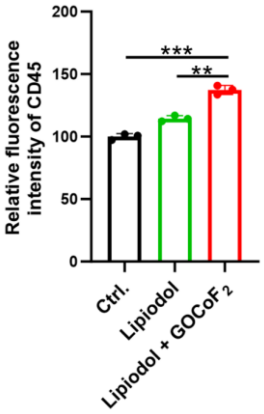

Figure S31. Quantitative analysis of the fluorescence intensity of CD45 in tumor tissues after various treatments.